J. Chem. Sci. (2019) 131:37
https://doi.org/10.1007/s12039-019-1613-x

REGULAR ARTICLE

Deformation of E_4 (E = P, As, Sb) tetrahedron structures *via* doping two atoms with elements from group 13: a study of the pseudo-Jahn–Teller effect

ALI REZA ILKHANI[a,b,*]

[a]Department of Chemistry, Yazd Branch, Islamic Azad University, Yazd, Iran
[b]Department of Chemistry, University of Alberta, Edmonton, AB T6G 2G2, Canada
E-mail: ilkhaniali@iauyazd.ac.ir

MS received 9 January 2019; revised 22 February 2019; accepted 3 March 2019; published online 2 May 2019

Abstract. White phosphorus and yellow arsenic are the most famous inorganic four-membered tetrahedral molecules in nature. Due to the recent application of the tetrahedron-based system as a carrier in drug delivery, the manipulation of the E_4 (E = P, As, Sb) tetrahedron structure by replacing two of the E atoms by elements from group 13 (D = Al, Ga, In) has been computationally explored. The symmetry-breaking phenomenon induced by the pseudo-Jahn–Teller effect was reported in the E_2D_2 tetrahedral structure. State averaging of the four low-lying electronic states along the a_2 deformation normal coordinate for the series in CASSCF(4,4)/cc–pVTZ–(PP) was carried out to formulate the $(1A_1 + 2A_1 + 1A_2) \otimes a_2$ PJTE problem and their corresponding coupling constants estimated by fitting the obtained state energies. Moreover, the deformed C_{2v} tetrahedral configuration of E_2D_2 can be restored by *i*) the protonation of the D atoms or *ii*) trapping a noble gas dication in the center cavity cage of the systems. Furthermore, the calculated thermodynamic properties of the E_2D_2 show that the protonation reaction acts as a spontaneous process fulfilling the $\Delta G < 0$ conditions and the considered series obeys the Bronsted–Lowry base behaviors.

Keywords. Pseudo-Jahn–Teller interaction; APES; electronic state mixing; deformed tetrahedron.

1. Introduction

An important aspect of drug delivery relies on dosage control and managing the side effects. A portion of this can be circumvented with the use of nano drug carriers. This can help combat the issues of drug resistance and uptake inefficiencies common in conventional deployment. The tetrahedron is one of the stable platonic structures in chemistry that are being paid recent attention in DNA tetrahedron-based drug delivery systems.[1] The presence of a cavity cage in the P_4 (E = P, As, Sb) tetrahedron systems makes them interesting as carriers of other substances in the field of computational chemistry. Despite the high angle strain found in tetrahedrons, white phosphorus (P_4) and yellow arsenic (As_4) are existing tetrahedral allotropes of P and As. Even for the element phosphorus, the P_4 tetrahedron is defined as the standard state.

The decomposition constant of the P_4 tetrahedron into two P_2 in the gas phase was experimentally tracked[2] and the high-temperature instability and photoelectron spectrum of the P_4^+ and As_4^+ tetrahedron were investigated.[3] The P_4 tetrahedron is an air-sensitive hydrophobic system that can be quelled by encapsulating it in a tetrahedral assembly of iron (II) ions and short organic chains.[4] The P_4 tetrahedron and the P_8 cubic structures have been computed and the phosphorus strain rings between them were compared.[5,6] The MNDO calculation was employed to show stability in the P_4 tetrahedron as well as the forbidden dissociation from the T_d to the D_{2d} symmetry.[7] Although the P_8 cubic structure has not been identified as a stable P allotrope, yet in reality, the MNDO calculations displayed that the P_8 cubical structure is more stable than the P_4 tetrahedron in gaseous media.[8] The decomposition pathway from P_4 to P_2 has been studied through calculating thermochemical properties as well as a thermal and photolysis reaction.[9–11]

The Jahn-Teller (JT) problem has been treated for the P_4^+ tetrahedral structure and the linear coupling constant for E_4^+ (E = P, As, Sb) corroborated with the experimental spectra.[12] Moreover, the combination of

*For correspondence

JT and pseudo-Jahn-Teller effects (PJTE) of the P_4^+ tetrahedral structure was studied by Koppel[13] and the JT effect of P_4^+ tetrahedral structure was formulated as $^2T_2 \otimes (t_{2+}\ e)$ problem.[14]

The PJTE is the only source to explain the origin of structural instability and spontaneous symmetry breaking in any unstable symmetrical system.[15,16] It was specifically employed to answer why some systems in their high-symmetry are unstable and deform to lower-symmetry stable structures, called symmetry breaking phenomena, in several types of research.[17–24] The PJTE has also been applied to rationalize the reason for instability in two-dimensional materials[25–29] as well as tracking the origin of puckering in unstable planar systems.[30–32] Another application of the PJTE is to find a way to restore the planarity of distorted molecules. To do this, nonplanar puckered molecules were coordinated by rings, atoms, or ions, which suppresses the PJTE in complexed systems.[33–38]

2. Methods and computational details

Due to the importance of accurate structural models of carriers in drug delivery, with the goal of understanding parameters that may affect carrier structure, the E_4 (E = P, As, Sb) tetrahedron were manipulated by replacing two of the E atoms from group 13 elements (D = Al, Ga, In) and the resulting E_2 D_2 tetrahedral structure has been computationally explored. Geometry optimizations and follow up frequency calculations for both the tetrahedron C_{2v} symmetry and deformed (C_2) configurations in all E_2D_2 considered systems were accomplished using the density functional theory with the B3LYP method[39] at the cc–pVTZ[40–42] basis set. Whereas Sb and In atoms are restricted in the cc–pVTZ basis set, the cc-pVTZ–PP pseudopotential basis set[43–45] is used instead in the computation of the Sb_2Al_2 and P_2In_2 systems. The state average-complete active space self–consistent field (SA–CASSCF) wave-function method[46–48] was employed to compute the ground and low-lying excited states along the a_2 deformation normal coordinate and to provide corresponding adiabatic potential energy surface (APES) cross-sections. According to the frequency calculations of the E_2D_2 systems, the four active electrons and four active orbitals that composes the CAS(4,4) active space was chosen on account of rationalizing electronic configurations, molecular orbital energies and symmetry elements of the systems. The MOLPRO 2015 package[49] carried out all computations in this article.

3. Results and Discussion

3.1 *Tetrahedral and deformed configurations*

Initially, the E_4 (E = P, As, Sb) tetrahedron structure was manipulated by replacing two vertices with Al atoms with geometry optimization and following frequency calculations for E_2Al_2 (E = P, As, Sb) series computed. An imaginary frequency along a_2 normal coordinate was observed for E_2Al_2. It was proven that the considered systems are unstable in their tetrahedral C_{2v} configuration. Indeed, observing the imaginary frequency in E_2Al_2 series points to the occurrence of the symmetry breaking phenomena (SBP) from C_{2v} high symmetry to the equilibrium structure C_2 lower symmetry.

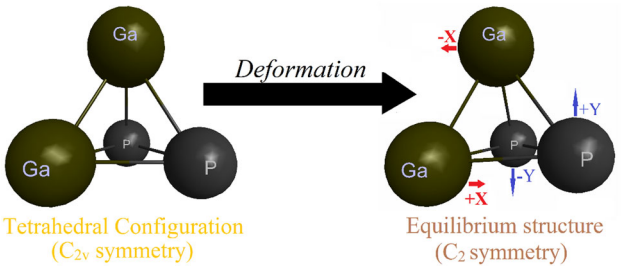

Figure 1. Illustration of the symmetry breaking phenomena and deformation of the C_{2v} tetrahedral configuration to the equilibrium structure with C_2 symmetry in P_2Ga_2 system.

Subsequently, Al atoms in E_2Al_2 series were replaced with other elements from group 13 along with geometry and frequency calculations. All E_2D_2 (E = P, As, Sb; D = Ga, In) systems with a tetrahedral structure show similarity in an imaginary frequency along the a_2 instability normal coordinate. Hence, P_2Ga_2, P_2In_2, and As_2Ga_2 were specifically explored due to their higher imaginary frequency values. The SBP from high–symmetry the C_{2v} tetrahedral configuration to the C_2 equilibrium structure for P_2Ga_2 as representative of the E_2D_2 systems are illustrated in Figure 1. Normal modes in X and Y Cartesian axis for Ga and P atoms are differentiated by different colors and directions.

To compare the effect of deformation in the E_2D_2 series under consideration, geometrical parameters in the form of bond lengths (Å), angles, and dihedral angles (degrees), imaginary frequencies (cm^{-1}), and dipole moment (Debye) for both unstable tetrahedral configurations (C_{2v} symmetry) and deformed equilibrium structures of the E_2Al_2 (E = P, As, Sb), P_2D_2 (D = Ga, In) and As_2Ga_2 systems are provided in Table 1.

Table 1 shows that all geometrical parameters in C_{2v} tetrahedral configuration change due to deformation in the E_2D_2 systems. Particularly, the E–D–E and D–E–D angles expand significantly from tetrahedral to deformed equilibrium structures in all compounds of the series. In addition, E–D–D–E and D–E–E–D dihedral angles also contract slightly from the C_{2v} to the C_2transition. Moreover, increasing the size of either E or D atoms in both of the manipulated E_2Al_2 and P_2D_2

Table 1. Geometry parameters, imaginary frequencies, normal modes, and dipole moment of E_2Al_2 (E = P, As, Sb), P_2D_2 (D = Ga, In) and As_2Ga_2 systems in unstable tetrahedral configuration (C_{2v} symmetry) and deformed equilibrium structure with C_2 lower symmetry.

Geometry parameters		P_2Al_2		As_2Al_2		Sb_2Al_2		P_2Ga_2		P_2In_2		As_2Ga_2	
		Tetrahedral (C_{2v})	Deformed (C_2)	Tetrahedral (C_{2v})	Deformed (C_2)	Tetrahedral (C_{2v})	Deformed (C_2)	Tetrahedral (C_{2v})	Deformed (C_2)	Tetrahedral (C_{2v})	Deformed (C_2)	Tetrahedral (C_{2v})	Deformed (C_2)
Bond length (Å)	E_1–E_2	2.399	3.189	2.535	3.282	2.810	3.662	2.459	3.279	2.682	3.720	2.596	3.592
	D_3–D_4		2.880		3.081		3.426		2.953		2.490		2.655
	E_1–D_4		2.295		2.402		2.618		2.323		2.521		2.863
	E_2–D_3												
	E_1–D_3		2.294		2.401		2.617		2.321		2.520		2.862
	E_2 – D_4												
Angle (deg)	E_1–E_2–D_3	60.00	45.97	60.00	46.89	60.00	47.21	60.00	45.08	60.00	42.43	60.00	44.83
	E_2–E_1–D_4												
	E_1–E_2–D_4		45.98		46.92		47.23		45.09		42.44		44.86
	E_2–E_1–D_3												
	E_1–D_3–E_2		88.04		86.19		83.84		89.84		90.12		89.88
	E_1–D_4–E_2												
	E_1–D_3–D_4		51.13		50.11		48.83		50.51		53.01		52.11
	E_2–D_4–D_3												
	E_1–D_4–D_3		51.11		50.08		48.82		50.52		53.04		53.13
	E_2–D_3–D_4												
	D_3–E_1–D_4		77.75		79.80		82.35		78.97		79.05		76.52
	D_3–E_2–D_4												
Dihedral angle (deg)	E_1–D_3–D_4–E_2	70.53	70.39	70.53	70.42	70.53	70.45	70.53	70.47	70.53	70.46	70.53	70.48
	E_2–D_3–E_1–D_4		67.23		67.86		68.24		67.89		68.25		68.80
	E_1–D_4–E_2–D_3												
	D_4–D_3–E_2–E_1		73.40		73.23		72.84		73.21		71.83		72.48
	D_3–D_4–E_1–E_2												
	D_3–E_1–E_2–D_4		70.40		70.47		70.50		70.42		70.44		70.48
Imaginary freq. (cm^{-1})		246.7	–	217.6	–	215.0	–	242.2	–	155.2	–	194.7	–
Normal modes in Cartesian	Y_D	±0.0995	–	±0.0420	–	±0.0273	–	±0.1057	–	±0.1128	–	±0.0567	–
	X_E	±0.0867		±0.1167		±0.1232		±0.0470		±0.0304		±0.0609	
Dipole moment (Debye)		3.26	2.66	2.89	2.48	2.10	2.03	2.72	2.20	3.46	2.63	2.40	1.62

Table 2. Main electronic configuration and their coefficients in the E_2Al_2 (E = P, As, Sb), P_2D_2 (D = Ga, In) and As_2Ga_2 systems.

State symmetry	Electronic configuration	Coefficients					
		P_2Al_2	As_2Al_2	Sb_2Al_2	P_2Ga_2	P_2In_2	As_2Ga_2
$1A_1$	$1a_1^2\ 1b_1^2$	0.9169	0.9399	0.8679	0.9360	0.9467	0.8687
	$1a_1^2\ 1a_2^2$	−0.0840	−0.0554	0.1571	−0.0184	−0.0857	0.2258
	$1b_1^2 1a_2^2$	−0.1726	−0.1490	−0.3999	−0.2414	−0.1956	−0.5389
$2A_1$	$1a_1^2\ 1b_1^2$	−0.0893	0.1032	0.4382	0.2027	0.1470	0.5888
	$1a_1^2\ 1a_2^2$	0.7351	−0.6537	−0.5456	−0.6100	−0.4865	−0.5232
	$1b_1^2 1a_2^2$	−0.6057	0.6793	0.6657	0.7089	0.5751	0.8041
$1B_1$	$1a_1^2\ 1b_1^1 1a_2^{-1}$	0.6453	0.6482	0.6644	0.6297	0.6678	0.6720
	$1a_1^2\ 1b_1^1 1a_2^{-1}$	−0.6453	−0.6482	−0.6644	−0.6297	−0.6678	−0.6720
	$1a_1^1\ 2a_1^1 1b_1^{-1} 1a_2^{-1}$	0.2019	0.1992	0.1758	0.1847	0.1721	0.1627
	$1a_1^{-1}\ 2a_1^{-1} 1b_1^1 1a_2^1$	0.2019	0.1992	0.1758	0.1847	0.1721	0.1627
$1A_2$	$1a_1^{-1}\ 1b_1^2 1a_2^1$	−0.5157	−0.5567	−0.6480	−0.6297	−0.6584	−0.6656
	$1a_1^1\ 1b_1^2 1a_2^{-1}$	0.5157	0.5567	0.6480	0.6297	0.6584	0.6656
	$1a_1^2\ 2a_1^1 1a_2^{-1}$	−0.3998	−0.3569	−0.2367	−0.2718	−0.2139	−0.2033
	$1a_1^2\ 2a_1^{-1} 1a_2^1$	0.3998	0.3569	0.2367	0.2718	0.2139	0.2033

series correspondingly increases the D–E–D angles as opposed to the imaginary frequency magnitude, as well as the D–D–E–E dihedral angels, across both the series. Furthermore, the dipole moment value decreases from the C_{2v} tetrahedral configuration to the C_2 equilibrium structure in all the E_2D_2 systems.

Hence, the size of an atom is a very important factor in the chemical behavior of its included systems, thereby requiring the effect of atoms size in deformation of the E_2D_2 series to be explored. Due to the imaginary frequency magnitudes in Table 2, when P atoms instead with larger atoms (As or Sb) are explored, the instability in the E_2Al_2 series decreases from 246.7 to 215.0 cm^{-1}. In a similar way, replacing Al by Ga and In atoms reduced the imaginary frequency to 242.2 and 155.2 cm^{-1} in P_2Ga_2 and P_2In_2 systems, respectively (except in the P_2Ga_2 and As_2Ga_2 series, in which it is the opposite).

3.2 *Electron configurations and excitation*

Electronic calculations were done for the $1A_1$ ground state and three low–lying excited states ($1B_1$, $2A_1$, $1A_2$) corresponding to the tetrahedral configuration of the considered E_2D_2 series. Here, 2, 1 and −1 superscripts denote pair–electrons and an electron in different orientations, respectively. Whereas, 1 and 2 prefixes indicate the first and second orbitals in similar symmetry. The main electronic configurations and their related coefficients for the mentioned states are provided in Table 2.

Table 2 shows that the highest coefficient in the $1A_1$ ground state belongs to the $1a_1^2\ 1b_1^2$ electronic configuration which indicates that four active electrons are placed in the HOMOs with a_1 and b_1 symmetries. Additionally, the $1a_1^{-1}\ 1b_1^2 1a_2^1$ and $1a_1^1\ 1b_1^2 1a_2^{-1}$ in the $1A_2$ excited state electronic configurations demonstrate an electron excitation from HOMO with a_1 symmetry to a LUMO with a_2 symmetry. By tracking the symmetry of the orbitals in the electronic configurations, only two LUMOs with a_1 and a_2 symmetries contributed in the electron configurations. In the other words, two HOMOs ($1a_1$, and $1b_1$) with two LUMOs ($2a_1$, and $1a_2$) compose the (4,4) active space that was employed in the SA–CASSCF calculations of the $1A_1$ ground and three $1B_1$, $2A_1$, $1A_2$, low–lying excited states in the E_2D_2systems.

Comparing the molecular orbital energies in the series to find the similarities in their electronic configurations guides us to choose an appropriate active state for the CASSCF calculation. This helps to reduce the number of independent parameters of the calculation in the study. Consequently, based on observed symmetry breaking phenomena from a C_{2v} tetrahedral configuration to the equilibrium structure with C_2 symmetry, an active space that at least concludes an a_1 and an a_2 in the HOMOs and LUMOs should be chosen for the calculation. Indeed, the chosen active space must have potential with a sufficient electron excitation, which matches with the PJTE in the series. Whereas in the systems under consideration, the HOMO and HOMO−1 are in a_1 and b_1 while the LUMO and LUMO+1 are in a_2 and a_1 symmetries

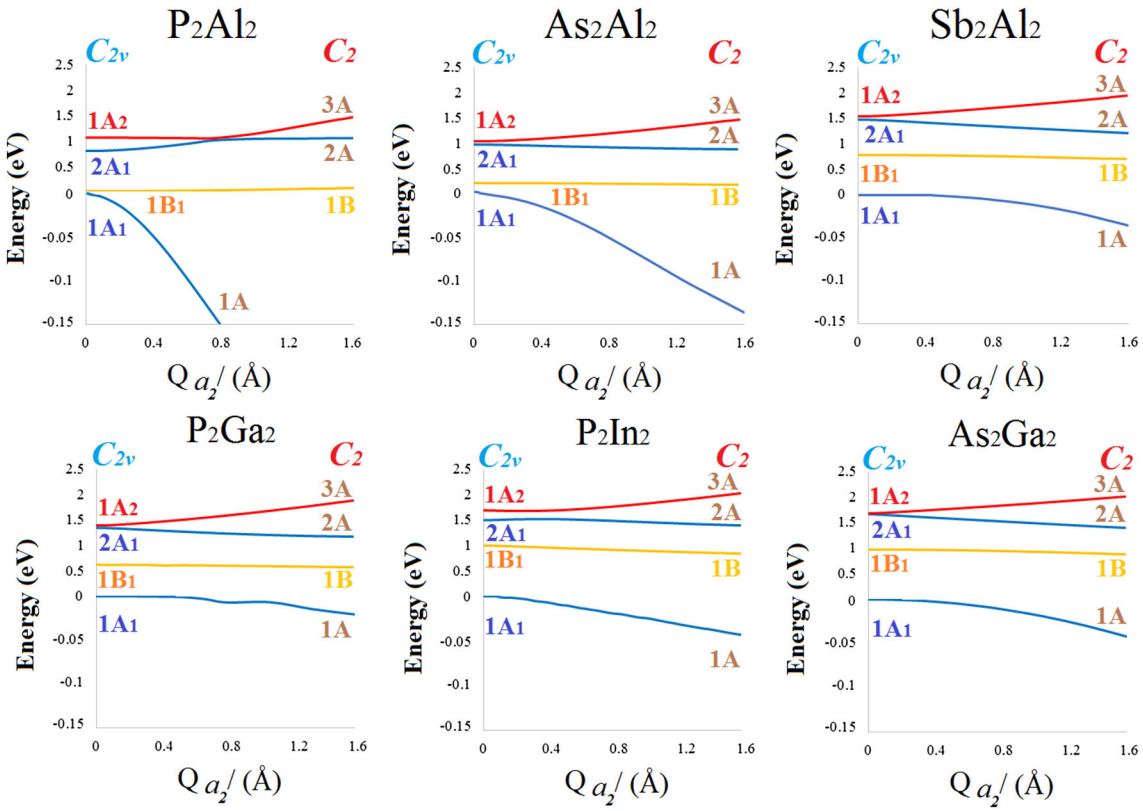

Figure 2. The adiabatic potential energy surface cross-sections (in eV) for the E_2Al_2 (E = P, As, Sb), P_2D_2 (D = Ga, In) and As_2Ga_2 systems along the Q_{a_2} instability directions. Note the changing energy scale in the profiles.

that justify why four electrons in four active orbitals are suitable for this study.

3.3 *Adiabatic potential energy cross-sections*

Based on observations of an electron excitation from a_1 to a_2 molecular orbitals, and regarding the normal modes of the imaginary frequencies of the E_2D_2 series oriented in the a_2 direction that was given in Table 1, the origin of the SBP in the series is a PJTE $(1A_1 + 1A_2) \otimes a_2$ problem. In other words, the SBP in the E_2D_2 series is caused by mixing the unstable $1A_1$ ground state with negative curvature and a stable low-lying A_2 excited state which should show a positive curvature along the a_2 normal coordinate. State averaging CASSCF calculations *via* the (4,4) active space were accomplished for the ground ($1A_1$), and low-lying excited ($2A_1$, $1B_1$, and $1A_2$) states corresponding to the E_2D_2 series considered. The obtained adiabatic potential energy surface (APES) cross-sections of the energy states around the Q_{a_2} instable directions were illustrated in Figure 2.

The APES cross sections in Figure 2 reveals that all considered E_2D_2 (E = P, As, Sb) systems are unstable in their $1A_1$ ground state, which is shown by a negative curvature, from tetrahedral C_{2v} configuration to deformed C_2 structure. Additionally, the $1A_2$ excited state demonstrates stability along the Q_{a_2} that corroborates with the condition of effective mixing between states *via* the expected PJTE $(1A_1 + 1A_2) \otimes a_2$ problem. The symmetry of the A_1, and A_2 states in C_2 deformed structure in all E_2D_2 series is A symmetry. Thus, any other low-lying excited states with a similar symmetry that is placed lower than $1A_2$ states in the APES must be added in the $(1A_1 + 1A_2 + \cdots) \otimes a_2$ PJTE problem. Hence, the second excited state in Figure 2 has an A_1 symmetry. It should be contributed as a modified form of the $(1A_1 + 2A_1 + 1A_2) \otimes a_2$ PJTE problem. Although, the first excited sate ($1B_1$) is located between the $2A_1$ and $1A_2$, it is specifically very close to the $1A_1$ ground state in the P_2Al_2, due to its B symmetry and is not to be added in the problem.

3.4 *The pseudo Jahn-Teller effect due to deformation*

Following the procedure of the general theory that has been introduced by Bersuker,[15,16] the wavefunction of the ground and two low-lying excited states with A symmetry were assumed as $|1A_1\rangle$, $|2A_1\rangle$ and $|1A_2\rangle$ and the interval energies between the $1A_1$ ground and $2A_1$ and $1A_2$ excited states by the Δ and Δ', respectively. Thus,

Table 3. The second order corrections, $K_1 - p_1$, $K_2 - p_2$, and $K_3 - p_3$; the PJTE coupling constants, F, and G; and interval energies Δ, Δ' for the E_2Al_2 (E = P, As, Sb), P_2D_2 (D = Ga, In) and As_2Ga_2 systems series obtained by fitting Equation (7) to the calculated the APES profiles in Figure 2.

Systems	$K_1 - p_1\left(\frac{eV}{Å^2}\right)$	$K_2 - p_2\left(\frac{eV}{Å^2}\right)$	$K_3 - p_3\left(\frac{eV}{Å^2}\right)$	$F\left(\frac{eV}{Å}\right)$	$G\left(\frac{eV}{Å}\right)$	$\Delta\ (eV)$	$\Delta'\ (eV)$
P_2Al_2	2.14	5.05	2.09	1.99	4.12	0.80	1.07
As_2Al_2	1.78	−0.59	1.92	1.85	−2.11	0.97	1.03
Sb_2Al_2	1.31	−1.48	1.63	1.72	−1.16	1.46	1.52
$:P_2Ga_2$	1.10	−1.63	1.84	1.88	−1.93	1.34	1.39
P_2In_2	1.43	−1.11	1.45	1.61	−1.44	1.48	1.68
Ga_2As_2	1.29	−1.70	1.64	1.69	−1.63	1.65	1.66

the $(1A_1 + 2A_1 + 1A_2) \otimes a_2$ PJTE problem makes the $1A_1$ ground state unstable and the necessary condition of instability around the Q_{a_2} normal coordinate yield in Equation (1):

$$\Delta' < \frac{F^2}{K_3 - p_3} \tag{1}$$

And the secular matrix equation of the problem is formulated as Equation (2):

$$\begin{vmatrix} \frac{(K_1-p_1)}{2}Q^2-\varepsilon & 0 & FQ \\ 0 & \frac{(K_2-p_2)}{2}Q^2+\Delta-\varepsilon & GQ \\ FQ & GQ & \frac{(K_3-p_3)}{2}Q^2+\Delta'-\varepsilon \end{vmatrix} = 0 \tag{2}$$

where, primary force constants and the vibronic coupling constants are K_1, K_2, K_3 (for $1A_1$, $2A_1$, $1A_2$) and F, G, respectively. Those mentioned constants can be introduced in the following Equations (3) and (4).

$$\begin{aligned} K_1 &= \langle 1A_1 | \left(\partial^2 H/\partial Q^2\right)_0 | 1A_1 \rangle, \\ K_2 &= \langle 2A_1 | \left(\partial^2 H/\partial Q^2\right)_0 | 2A_1 \rangle, \\ K_3 &= 1\langle A_2 | \left(\partial^2 H/\partial Q^2\right)_0 | 1A_2 \rangle \end{aligned} \tag{3}$$

$$\begin{aligned} F &= \langle 1A_1 | \left(\partial H/\partial Q\right)_0 | 1A_2 \rangle, \\ G &= \langle 2A_1 | \left(\partial H/\partial Q\right)_0 | 1A_2 \rangle \end{aligned} \tag{4}$$

In addition, H is electronic Hamiltonian with respect to the Q_{a_2} instability direction and p_1, p_2, p_3 are the second-order perturbation corrections from all the higher excited A symmetry states to $1A_1$, $2A_1$, $1A_2$ states, respectively. These perturbation corrections are given by Equation (5):

$$\begin{aligned} -2\sum_n \frac{|F_{1n}|^2}{E_n - E_1} {Q_{a_2}}^2 &= -p_1 {Q_{a_2}}^2, \\ -2\sum_n \frac{|F_{2n}|^2}{E_n - E_2} {Q_{a_2}}^2 &= -p_2 {Q_{a_2}}^2, \\ -2\sum_n \frac{|F_{3n}|^2}{E_n - E_3} {Q_{a_2}}^2 &= -p_3 {Q_{a_2}}^2 \end{aligned} \tag{5}$$

Here, F_{1n}, F_{2n}, F_{3n} are referred to as the vibronic coupling constants between the $1A_1$ $2A_1$, $1A_2$ (as first, second, third A symmetry) states and the n high–energy excited state and E is corresponded to their energies.

The 3×3 secular Equation (2) can be simplified by using f, g, a, b, and c denotations to Equation (6).

$$\begin{vmatrix} a-\varepsilon & 0 & f \\ 0 & b-\varepsilon & g \\ f & g & c-\varepsilon \end{vmatrix} = 0 \tag{6}$$

After the Equation (6) expansion, the mathematical solutions are provided as Equation (7).

$$\begin{cases} \varepsilon_1 + \varepsilon_2 + \varepsilon_3 = a + b + c \\ \varepsilon_1\varepsilon_2 + \varepsilon_2\varepsilon_3 + \varepsilon_1\varepsilon_3 = ab + ac + bc - f^2 - g^2 \\ \varepsilon_1\varepsilon_2\varepsilon_3 = abc + cf^2 + bg^2 \end{cases} \tag{7}$$

According to the $(1A_1+2A_1+1A_2)\otimes a_2$ problem in E_2D_2 systems, f, g, a, b, and c variables were fitted from the obtained energies in the APES cross-sections profiles in Figure 2 and their related PJTE coupling constants (F and G), as well as of the perturbation corrected force constant parameters ($K_1 - p_1$, $K_2 - p_2$, and $K_3 - p_3$) were estimated and revealed in Table 3.

3.5 *Restoring tetrahedral structure*

With the goal of restoring the tetrahedral structure and quenching the PJTE in the E_2D_2 systems under consideration, protonation of D atoms and trapping a noble gas dication at the center of the cavity cage of the systems were explored and the plausibility of these methods was examined.

3.5a *Protonation of D atoms*: In the first effort of suppressing the PJTE, two protons (H^+) are placed at the apexes of the E_2D_2 deformed tetrahedral pyramid (same as the positions that hydrogens located in tetrahedrane structure). The geometrical optimization and frequency calculation of the simulated $E_2D_2H_2^{2+}$ revealed that the complexes restore their C_{2v} tetrahedral configuration

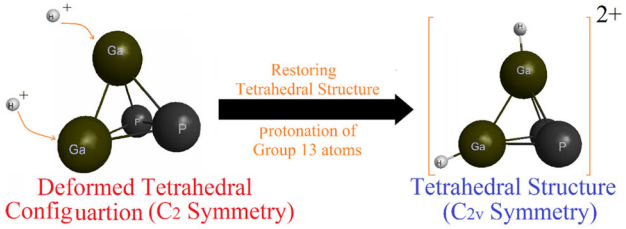

Figure 3. Representative of restoring the Ga_2P_2 tetrahedral structure (C_{2v} symmetry) from the deformed configuration with C_2 symmetry through the protonation of Ga atoms. Other E_2D_2 deformed systems considered also demonstrate that the $E_2D_2H_2^{2+}$ complexes restoration.

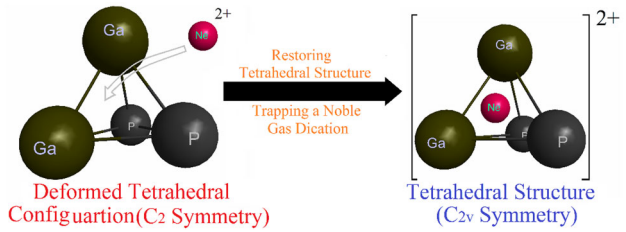

Figure 4. Representative of restoring the Ga_2P_2 tetrahedral structure (C_{2v} symmetry) from the deformed configuration with C_2 symmetry through trapping Ne^{2+} inside the tetrahedron cage. Other deformed In_2P_2 and Ga_2As_2 configurations demonstrate analogous restoration with Ne^{2+} or He^{2+}.

without a disrupted structure (Figure 3) and do not show any imaginary frequency.

In addition, the calculated thermochemical parameters at standard temperature and pressure for the protonation reaction in the considered E_2D_2 systems return a negative ΔG value from –12.45 KJ/mol in P_2Al_2 to –5.83 KJ/mol in P_2In_2. In fact, the E_2D_2 protonation process, as well as the formation of the $E_2D_2H_2^{2+}$ complexes is a spontaneous reaction, thermodynamically.

Based on the general definition of Bronsted-Lowry, a base refers to the compound that behaves as an H^+ proton acceptor. Although group 13 elements are potentially familiar with accepting electron-pairs (Lewis acid concept), the E_2D_2 systems become stable by protonation of the D atoms in the $E_2D_2H_2^{2+}$ complexes which are in conflict with our expectations.

3.5b *Trapping noble gas dication inside E_2D_2 cage*: In the second attempt to quenching the PJTE, $He^{2+}$and Ne^{2+} were trapped in the center hole of the E_2D_2 systems. No imaginary frequency was observed for $He^{2+}@E_2D_2$ or $Ne^{2+}@E_2D_2$ cages, from the optimization and following frequency calculations (see the $Ne^{2+}@P_2Ga_2$ trapped system illustrates in Figure 4). Consequently, the PJTE in the $He^{2+}@E_2D_2$ or $Ne^{2+}@E_2D_2$ cages was suppressed and the E_2D_2 systems restore their tetrahedral structure.

As was mentioned in Equation (1), Δ' must be less than $\frac{F^2}{K_3-p_3}$, as the necessary condition for instability of the ground state in the series. By both the trapping of an inert gas dication and the di-protonation efforts for E_2D_2 series, the interval energies between the $1A_1$ ground and all three, low–lying excited states ($1B_1$, $2A_1$, $1A_2$) changes. Specifically, the energy gap between the ground and A_2 excited states, Δ', is significantly increased. For examples, the Δ' in the E_2Al_2 (E = P, As, Sb) series increases from 1.07, 1.03, 1.57 eV to 5.86, 5.76, 3.46 when trapping He^{2+} ($He^{2+}@E_2Al_2$) and 7.32, 6.02, 4.94 eV with Al atoms di-protonated ($E_2Al_2H_2^{2+}$). Therefore, increasing the magnitude of Δ' increases stability in the A_1 ground state, quenching the PJTE in the E_2Al_2 systems.

However, di-protonation to E atoms in E_2Al_2 (E = P, As, Sb) series increases the value of the imaginary frequencies in the series from 246.7, 217.6, and 215.0 to 448.4, 409.0, and 421.9 cm^{-1}. In other words, protonating E atoms of E_2Al_2 will increase the PJTE, the instability of C_{2v} tetrahedral configuration, in the series. To explain the reason, exploring the molecular orbital energies of E_2Al_2 and di-protonated to Al atoms ($H_2^{2+}E_2Al_2$) complexes is useful. Due to the number of electrons in the P_2Al_2, $P_2Al_2H_2^{2+}$ and $He^{2+}@E_2Al_2$ systems being the same, all of these follow the same configuration of $12a_1$, $7b_1$, $6b_2$, $3a_2$ HOMOs. In the $H_2^{2+}P_2Al_2$ system, however, the HOMOs rearrange as $12a_1$, $7b_1$, $5b_2$, $4a_2$. Here, the highest electron pair in the b_2 symmetry change to a_2 symmetry electrons. In other words, the electronic configuration in $H_2^{2+}P_2Al_2$ is different with respect to P_2Al_2, $P_2Al_2H_2^{2+}$ and $He^{2+}@E_2Al_2$ systems and thus, the energy gap between the highest a_1 HOMO and a_2 LUMO is affected. Similarly, in the di-protonation of P in P_2Al_2 system, $H_2^{2+}E_2Al_2$ (E = As, Sb) also show re-arrangement between the b_2 and a_2 symmetries HOMO electrons.

4. Conclusions

According to the application of tetrahedron structures as a carrier in drug delivery and toward developing efficiency in targeted drugs, the manipulation of white phosphorus and its family group series E_4(E = P, As, Sb) were explored by replacing two E atoms by group 13 (D) elements. Consequences of the state averaging CASSCF calculations, electron excitation, and the corresponded APES reveal that the $(1A_1+2A_1+1A_2)\otimes a_2$ problem is the reason for the origin of deformation, as well as the symmetry breaking phenomena, in the E_2D_2 systems. Moreover, calculation results present the protonation of the D atoms and trapping a noble gas dication in center

of the cage in the systems as two successful efforts for restoring the tetrahedral structure and suppressing the PJTE in the E_2D_2 systems.

Acknowledgements

The author wishes to acknowledge the Yazd Branch, Islamic Azad University for their financial support in the research. This work has been enabled in part with support provided by Dr. Alex Brown (University of Alberta), Westgrid (www.westgrid.ca), and Compute/Calcul Canada (www.computecanada.ca).

References

1. Hu Y, Chen Z, Zhang H, Li M, Hou Z, Luo X and Xue X 2017 Development of DNA tetrahedron-based drug delivery system *Drug Deliv.* **24** 1295
2. Corbridge D E C 1974 In *Structural Chemistry of Phosphorus* (Amsterdam: Elsevier) p. 12
3. Wang L S, Niu B, Lee Y T, Shirley D A, Ghelichkhani E and Grant E R 1990 Photoelectron spectroscopy and electronic structure of clusters of the group V elements. III. Tetramers: The $^2T_2$ and $^2A_1$ excited states of P^+_4, As^+_4, and Sb^+_4 *J. Chem. Phys.* **93** 6327
4. Mal P, Breiner B, Rissanen K and Nitschke J R 2009 White phosphorus is air-stable within a self-assembled tetrahedral capsule *Science* **324** 1697
5. Ahlrichs R, Brode S and Ehrhardt C 1985 Theoretical study of the stability of molecular P_2, P_4 (T.alpha.), and P_8 (O_h) *J. Am. Chem. Soc.* **107** 7260
6. Kutzelnigg W 1984 Chemical bonding in higher main group elements *Angew. Chem. Int. Ed.* **23** 272
7. Bock H and Muller H 1984 Gas-phase reactions. 44. The phosphorus P_4 .dblarw. $2P_2$ equilibrium visualized *Inorg. Chem.* **23** 4365
8. Schmidt M W and Gordon M S 1985 Observability of cubic octaphosphorus *Inorg. Chem.* **24** 4503
9. Karton A and Martin J M 2007 W4 thermochemistry of P_2 and P_4. Is the CODATA heat of formation of the phosphorus atom correct? *Mol. Phys.* **105** 2499
10. Wang L P, Tofan D, Chen J, Van Voorhis T and Cummins C C 2013 A pathway to diphosphorus from the dissociation of photoexcited tetraphosphorus *RSC Adv.* **3** 23166
11. Oakley M S, Bao J, Klobukowski M, Truhlar D G and Gagliardi L 2018 Multireference methods for calculating the dissociation enthalpy of tetrahedral P_4 to two P_2 *J. Phys. Chem. A* **122** 5742
12. Wang L S, Niu B, Lee Y T, Shirley D A, Ghelichkhan E and Grant E R 1990 Photoelectron spectroscopy and electronic structure of clusters of the group V elements. II. Tetramers: Strong Jahn–Teller coupling in the tetrahedral ^2E ground states of P^+_4, As^+_4, and Sb^+_4 *J. Chem. Phys.* **93** 6318
13. Meiswinkel R and Koppel H 1992 Combined Jahn–Teller and pseudo-Jahn–Teller effects in the P_4+ cation *Chem. Phys. Lett.* **201** 449
14. Bhattacharyya S, Opalka D and Domcke W 2015 E × e Jahn–Teller effect in the $P_4{}^+$ cation and its signatures in the photoelectron spectrum of P_4 *Chem. Phys.* **460** 51
15. Bersuker I B 2006 *The Jahn–Teller Effect* (Cambridge: Cambridge University Press) p. 110
16. Bersuker I B 2013 Pseudo Jahn–Teller effect—A two-state paradigm in formation, deformation, and transformation of molecular systems and solids *Chem. Rev.* **113** 1351
17. Blancafort L, Bearpark M J and Robb M A 2006 Ring puckering of cyclooctatetraene and cyclohexane is induced by pseudo-Jahn–Teller coupling *Mol. Phys.* **104** 2007
18. Liu Y, Bersuker I B, Garcia-Fernandez P and Boggs J E 2012 Pseudo Jahn–Teller origin of nonplanarity and rectangular-ring structure of tetrafluorocyclobutadiene *J. Phys. Chem. A* **116** 7564
19. Hermoso W, Ilkhani A R and Bersuker I B 2014 Pseudo Jahn–Teller origin of instability of planar configurations of hexa-heterocycles $C_4N_2H_4X_2$ (X = H, F, Cl, Br) *Comput. Theor. Chem.* **1049** 109
20. Soto J R, Molina B and Castro J J 2015 Reexamination of the origin of the pseudo Jahn–Teller puckering instability in silicene *Phys. Chem. Chem. Phys.* **17** 7624
21. Ilkhani A R, Hermoso W and Bersuker I B 2015 Pseudo Jahn–Teller origin of instability of planar configurations of hexa-heterocycles. Application to compounds with 1,2– and 1,4–C_4X_2 skeletons (X = O, S, Se, Te) *Chem. Phys.* **460** 75
22. Liu Y, Bersuker I B and Boggs J E 2013 Pseudo Jahn–Teller origin of puckering in $C_4H_2^{+2}$, $Si_4H_2^{+2}$, and $C_4F_2^{+2}$ dications *Chem. Phys.* **417** 26
23. Ilkhani A R 2015 Pseudo Jahn–Teller origin of twisting in 3, 6-pyridazinedione derivatives; $N_2C_4H_2Y_2Z_2$ (Y = O, S, Se, Z = H, F, Cl, Br) compounds *J. Theor. Comput. Chem.* **6** 1550045
24. Ilkhani A R 2019 The symmetry breaking phenomenon in heteronine analogues due to the pseudo Jahn–Teller effect *J. Mol. Model.* **25** 8
25. Gorinchoy N N, Arsene I and Bersuker I B 2018 Buckybowl structure of sumanenes and distortions of thiophenes induced by the pseudo Jahn–Teller Effect *J. Phys. Conf. Ser.* **1148** 012005
26. Ilkhani A R 2017 The symmetry breaking phenomenon in 1,2,3-trioxolene and $C_2Y_3Z_2$ (Z = O, S, Se, Te, Z = H, F) compounds: A pseudo Jahn–Teller origin study *Quim. Nova* **40** 491
27. Ilkhani A R and Monajjemi M 2015 The Pseudo Jahn–Teller effect of puckering in pentatomic unsaturated rings C_4AE_5, A = N, P, As, E = H, F, Cl *Comput. Theor. Chem.* **1074** 19
28. Bhattacharyya K, Surendran A, Chowdhury C and Datta A 2016 Steric and electric field driven distortions in aromatic molecules: Spontaneous and non-spontaneous symmetry breaking *Phys. Chem. Chem. Phys.* **18** 31160
29. Ilkhani A R 2017 Pseudo Jahn–Teller Effect in oxepin, azepin, and their halogen substituted derivatives *Russ. J. Phys. Chem. A* **91** 1743
30. Jose D and Datta A 2011 Structures and electronic properties of silicene clusters: A promising material for FET and hydrogen storage *Phys. Chem. Chem. Phys.* **13** 7304
31. Chowdhury C, Jahiruddin S and Datta A 2016 Pseudo-Jahn–Teller distortion in two-dimensional phosphorus: Origin of black and blue Phases of phosphorene and band

gap modulation by molecular charge transfer *J. Phys. Chem. Lett.* **7** 1288
32. Pratik S Md, Chowdhury C, Bhattacharjee R, Jahiruddin S and Datta A 2015 Psuedo Jahn–Teller distortion for a tricyclic carbon sulphide (C_6S_8) and its suppression in S-oxygenated dithiine ($C_4H_4(SO_2)_2$) *Chem. Phys.* **460** 101
33. Jose D and Datta A 2012 Understanding of the buckling distortions in silicene *J. Phys. Chem. C* **116** 24639
34. Ilkhani A R 2015 Pseudo Jahn–Teller origin of puckering in cyclohexahomoatomic molecules E_6 (S, Se, Te) and restoring S_6 planar ring configuration *J. Mol. Struct.* **1098** 21
35. Ivanov A S, Bozhenko K V and Boldyrev A I 2012 On the suppression mechanism of the pseudo-Jahn–Teller Effect in middle E_6 (E = P, As, Sb) rings of triple-decker sandwich complexes *Inorg. Chem.* **51** 8868
36. Pokhodnya K, Olson C, Dai X, Schulz D L, Boudjouk P, Sergeeva A P and Boldyrev A I 2011 Flattening a puckered cyclohexasilane ring by suppression of the pseudo-Jahn–Teller effect *J. Chem. Phys.* **134** 1
37. Sergeeva A P and Boldyrev A I 2010 Flattening a puckered pentasilacyclopentadienide ring by suppression of the pseudo Jahn–Teller effect *Organometallics* **29** 3951
38. Ilkhani A R, Gorinchoy N N and Bersuker I B 2015 Pseudo Jahn–Teller effect in distortion and restoration of planar configurations of tetra-heterocyclic 1,2-diazetes $C_2N_2E_4$, E = H, F, Cl, Br *Chem. Phys.* **460** 106
39. Polly R, Werner H J, Manby F R and Knowles P J 2004 Fast Hartree–Fock theory using local density fitting approximations *Mol. Phys.* **102** 2311
40. Wilson A K, Woon D E, Peterson K A and Dunning T H 1999 Gaussian basis sets for use in correlated molecular calculations. IX. The atoms gallium through krypton *J. Chem. Phys.* **110** 7667
41. Woon D E and Dunning T H 1993 Gaussian basis sets for use in correlated molecular calculations. III. The atoms aluminum through argon *J. Chem. Phys.* **98** 1358
42. Dunning T H 1989 Gaussian basis sets for use in correlated molecular calculations. I. The atoms boron through neon and hydrogen *J. Chem. Phys.* **90** 1007
43. Peterson K A 2003 Systematically convergent basis sets with relativistic pseudopotentials. II. Small-core pseudopotentials and correlation consistent basis sets for the post-d group 16–18 elements *J. Chem. Phys.* **119** 11099
44. Dolg M 1996 On the accuracy of valence correlation energies in pseudopotential calculations *J. Chem. Phys.* **104** 4061
45. Dolg M 1996 Valence correlation energies from pseudopotential calculations *Chem. Chem. Phys. Lett.* **250** 75
46. Werner H J and Meyer W 1981 A quadratically convergent MCSCF method for the simultaneous optimization of several states *J. Chem. Phys.* **74** 5794
47. Werner H J and Knowles P J 1985 A second order multiconfiguration SCF procedure with optimum convergence *J. Chem. Phys.* **82** 5053
48. Werner H J and Meyer W 1980 A quadratically convergent multiconfiguration-self-consistent field method with simultaneous optimization of orbitals and CI coefficients *J. Chem. Phys.* **73** 2342
49. Werner H J, Knowles P J, Manby F R and Schutz M 2015 MOLPRO, version 2015.1.22, a package of ab initio programs. http://www.molpro.net